Heavy Light

Nathan Mirman

November 8, 2013

1 Introduction

The past century of astrophysical observations has yielded a large body of evidence supporting the existence of dark matter (DM) in our universe. Measurements dating back to the early 1930s of galaxy rotation curves and the orbital velocities of galaxies within clusters have consistently shown a discrepancy between the amount of luminous matter and the total gravitational energy contained in these systems. Signatures of DM were also observed by measuring the gravitational lensing around galaxy clusters. Perhaps the most striking example is evident in the collision between two galaxy clusters known as the Bullet Cluster, where we see a separation between the baryonic matter and a large non-luminous mass which is visible only through gravitational lensing. Evidence for DM also comes indirectly from detailed measurements of the angular fluctuations in the Cosmic Microwave Background (CMB). A recent analysis of the CMB points to a universe consisting of only 5% ordinary matter, where the remaining content is due to 27% dark matter and 68% dark energy.

These striking developments have engendered a continued effort to reveal the identity of DM. Namely, if DM has a particle explanation, the goal is to describe its properties and observe it in terrestrial experiments. Theoretically, a favored candidate for DM is the weakly-interacting massive particle (WIMP) which emerges from various models in supersymmetry (SUSY), especially those which impose symmetries such as R-parity conservation. However, R-parity conserving SUSY is yet to be observed at the LHC, and many other theoretically-viable alternatives exist for physics beyond the standard model (SM).

In the last two decades, several surprising features have been observed in high-energy cosmic rays, as well as gamma-ray and microwave emissions from the galactic center. Recent results from direct DM searches DAMA/LIBRA and CDMS have shown excesses as well. When viewed collectively, these features motivate a *dark sector* explanation for dark matter which includes both particles and forces that are only loosely coupled to the SM. Here, we explore the experimental and theoretical motivations for a dark sector with an emphasis on dark photons. We discuss the theoretical properties of the dark photon as well as future experimental efforts to probe for its existence.

2 Experimental Motivations for a Dark Sector

Indirect evidence for DM has been obtained by a variety of experiments measuring e^+e^- cosmic ray spectra, as well as gamma ray and microwave emissions from vicinity of the galactic center. Signatures have also emerged from the direct detection experiments DAMA/LIBRA and CDMS. Along with theoretical considerations, these measurements make a strong case for a dark sector. Here we briefly outline the relevant details of these important experimental results.

2.1 Excess in High-Energy Cosmic Rays

Currently accepted models of cosmic ray production are based on the emission of *primary* cosmic ray protons and alpha particles from supernovae and other astrophysical sources, and their subsequent interaction with the interstellar medium (ISM) to produce *secondary* cosmic rays. The anti-matter particles found in cosmic rays are expected to fall into the latter category, and have a flux $\phi(e^+)$ which decays with increasing energy. Typically, the GALPROP code is used to simulate the production and propagation of cosmic ray particles and to estimate their spectra [1].

In 2008, PAMELA observed a clear excess in the positron fraction, $\phi(e^+)/(\phi(e^+) + \phi(e^-))$, at energies above 10 GeV [2]. This was later confirmed by the Fermi and AMS-02 experiments [3, 4]. The most recent results from these satellite-based experiments, shown in Figure 1(a), indicate a monotonically increasing positron fraction up to energies of several hundred GeV. The measured spectrum shows a significant deviation from GALPROP estimates, assuming the secondary production of cosmic ray positrons. No such excess in the anti-proton flux is observed. The measured excess been compared with models in which positrons are produced in DM interactions, and the resulting spectra fit the data quite well. Alternative astrophysical explanations include positron production from nearby pulsars, supernova remnants, and other astronomical objects.

In addition to the upturn observed in positron fraction at high-energies, the balloon-borne ATIC experiment has reported a peak-like excess in the $e^+ + e^-$ flux in the energy range 100 to 800 GeV (Figure 1(b)) [5]. This experiment cannot distinguish between positive and negative electrons, so the measurement is compared to the combined yield predicted by models of secondary production. The excess fits well to models which include DM annihilation into electrons.

2.2 Excess in Gamma Rays

The EGRET and INTEGRAL experiments have measured the spectra of gamma rays emanating from the galactic center [6, 7]. EGRET has observed an excess of diffuse gamma rays in the energy range 10-50 GeV, which can be explained by the inverse Compton scattering of e^+e^- off of starlight and the CMB. The INTEGRAL results show an excess at the 511 keV line over the rate expected from supernovae. This can result from the collisions of low-energy e^+e^- produced near threshold in the galactic center.

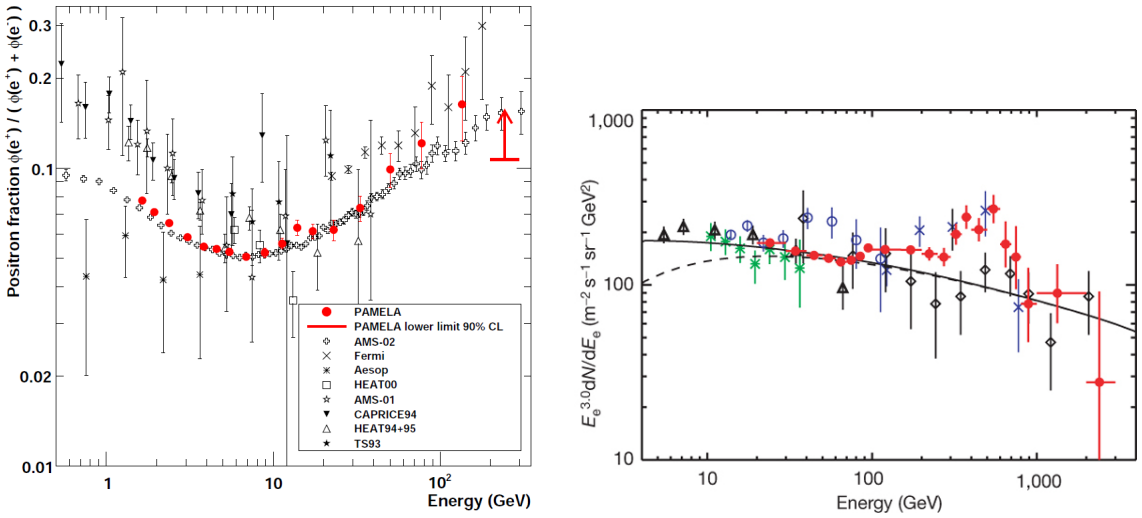

(a) (b)

Figure 1: Measured spectra of high-energy cosmic rays. In (a), measurements of the positron fraction from PAMELA and other experiments are shown. An excess is observed at energies above 10 GeV. The discrepancy between experiments below $\sim$ 10 GeV can be attributed to decade-long cycles in solar activity. Shown in (b) are the results from ATIC and other experiments on the electron flux. The solid and dashed lines indicate the expected spectrum obtained from GALPROP simulation.

2.3 WMAP Haze

The primary mission of the WMAP experiment is to obtain precise measurements of the CMB. However, the microwave *foreground* spectrum obtained from WMAP data shows structure which is not accounted for by any known astrophysical sources [8]. The WMAP data is collected in five frequency bands in the range 23-91 GHz. The known sources of foreground microwave emissions have spectra which are sampled by the five frequency bands, thus allowing their subtraction from the total. These include synchrotron radiation from electrons accelerated in supernovae, free-free radiation caused by the thermal bremsstrahlung of hot electron and ion gas, and emissions from thermal and spinning dust [8, 9]. Figure 2 demonstrates the results of a regression fit performed to model these contributions as they enter the total foreground emissions. In the first row, we have a foreground map where the CMB has been subtracted from the total microwave spectrum. The rightmost column shows a template that is obtained by combining the five frequency bands to the left. This template is then subtracted to obtain the map in the next row, and so on. After subtracting all known sources, the remaining WMAP haze is exposed in row 6. This haze can be interpreted as synchrotron radiation from electrons and positrons produced in DM interactions at the galactic center.

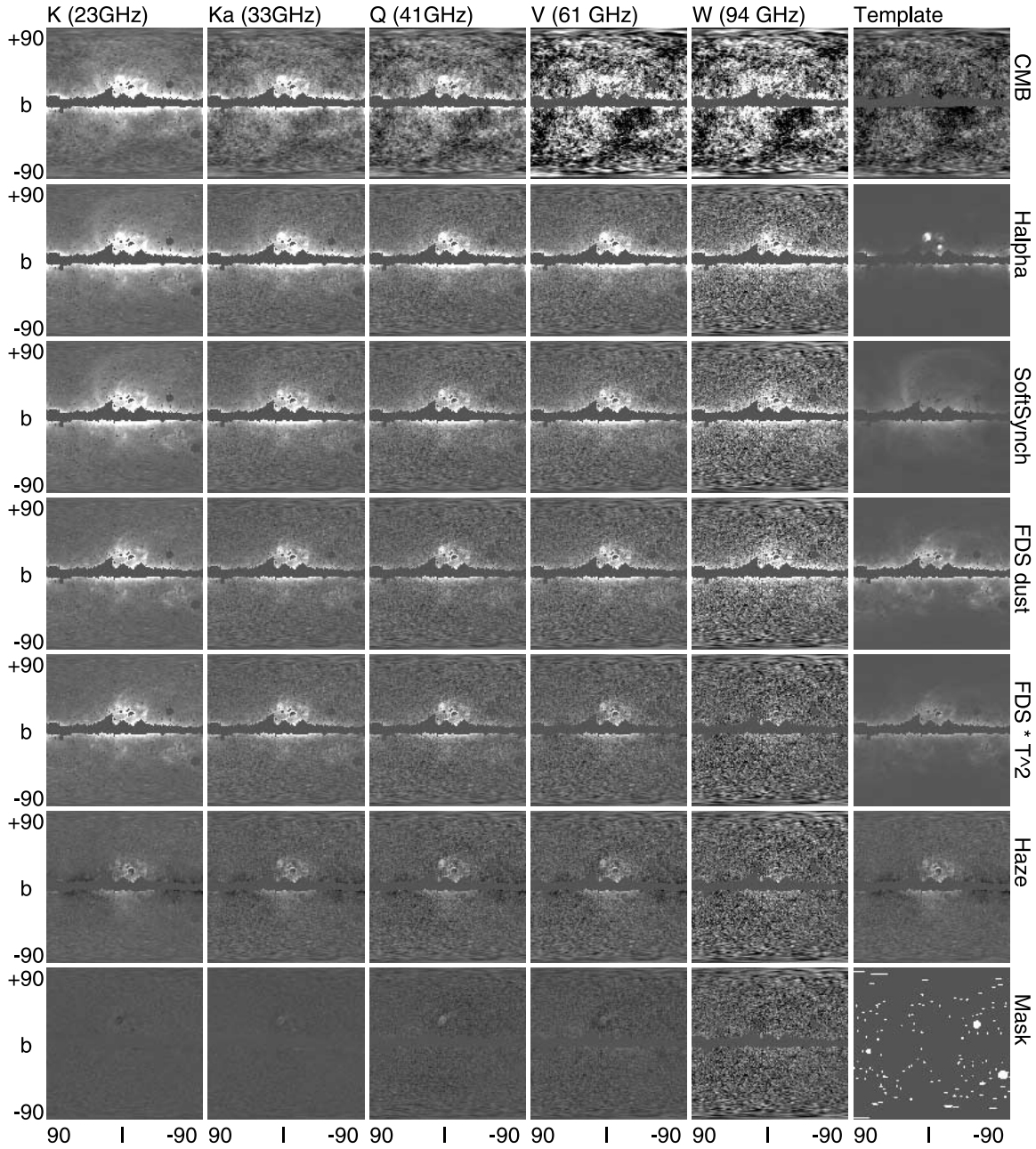

Figure 2: WMAP grid showing the contributions to the microwave foreground [8]. The WMAP haze is shown in the 6th row.

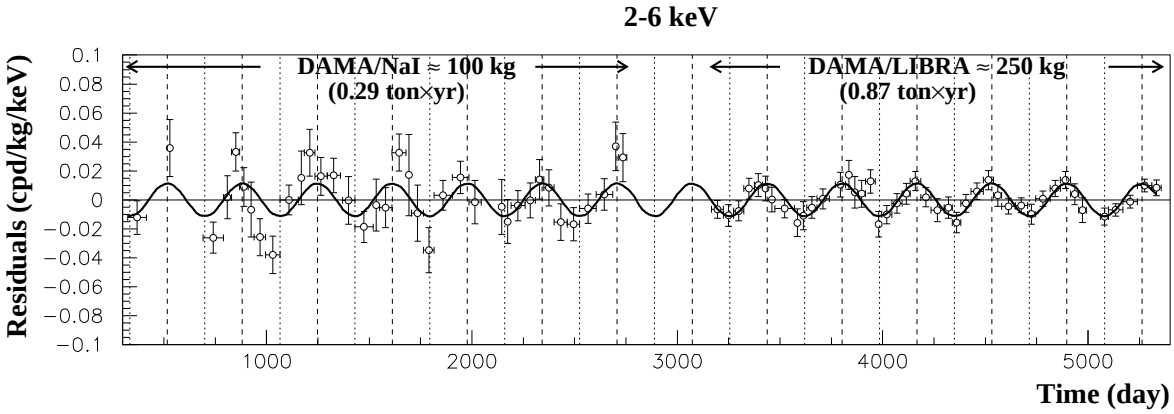

Figure 3: Results of the DAMA/NaI and DAMA/LIBRA experiments showing an annual modulation of hits. The line shown has a period of one year and a phase of 152.5 days corresponding to a maximum flux on June 2.

2.4 Direct Searches

Results from the DAMA/LIBRA experiment have shown an annual modulation in the rate of observed hits (Figure 3) [10]. Certain models of DM predict such a modulation due to the Earth's revolution around the Sun (and the Sun's motion inside the galaxy). Such models predict a maximum in the DM flux around June 2, when the Earth and the Sun move in phase with respect to the galactic center, and a minimum around Dec 2 when the Earth and the Sun move out of phase. These predictions agree with the DAMA/LIBRA observations. However, the interpretation of these results is complicated by the correlation of the observed modulation with the Earth's seasons.

Recently, the CDMS experiment has released results which contain three candidate DM events [11]. The probability of known backgrounds producing three events in the measurement's signal region is 5.4%. This probability decreases to 0.19% if the measured recoil energies are also taken into account. The CDMS results point to a WIMP of mass 8.6 GeV and WIMP-nucleon cross section of 1.9×10^{-41} cm^2.

3 Interpretation and Theory

The collection of evidence outlined above has strongly motivated a dark sector explanation for DM [12]. These facts have also provided some input on the properties of possible dark sector candidates. The excess observed in GeV-scale e^+e^- cosmic rays, along with indirect hints of e^+e^- production from measurements of gamma rays from the galactic center, must be reconciled with no apparent excesses in the production of hadrons. The anti-proton spectrum observed at PAMELA shows no deviations from GALPROP models, and measured gamma ray spectra set a limit on the $\pi^0\pi^0$ production by DM scattering. Thus, the DM interactions must have a large cross section for lepton production, but a small cross section for hadronic

final states. These considerations point to a particle of mass $2m_e \lesssim m \lesssim 2m_\pi$ which decays exclusively to leptons. One possible candidate for this particle is the dark photon A'.

A dark photon with MeV-scale mass can interact with a GeV-scale WIMP DM via $\chi\chi \to A'A'$. An interesting feature of this interaction arises when we attempt to reconcile the tension between the e^+e^- excess observed in cosmic rays with the small annihilation cross section allowed by thermal relic abundance. A solution to this dilemma, proposed in [12], utilizes the Sommerfeld enhancement resulting from a gauge boson of mass $m_{A'} \lesssim \alpha m_\chi \sim$ several GeV. The Sommerfeld enhancement is easily understood by analogy to the classical system of a point particle impinging on a star of radius R. Neglecting any interactions, we obtain a cross section $\sigma_0 = \pi R^2$. However, in the case of an attractive (gravitational) potential, a slow-moving particle is more likely to hit its target than a fast-moving one. The cross-section is now enhanced to $\sigma = \sigma_0(1 + v_{\rm esc}^2/v^2)$, where $v_{\rm esc}$ is the escape velocity of the particle in the attractive potential.

In the case of WIMP interactions $\chi\chi \to A'A'$, the A' can provide a Sommerfeld enhancement which 'turns on' in the low-velocity regime. In the early universe when the DM is in thermal equilibrium, the enhancement is negligible. However, in the era proceeding thermal freeze-out the DM particles have been redshifted to lower velocities, resulting in an $\mathcal{O}(100)$ boost to their interaction cross section. Such a scenario favors a relatively light A' ($m_{A'} \lesssim$ a few GeV), and additional constraints from big bang nucleosynthesis set a lower bound of approximately 10 MeV on its mass. This is again consistent with an A' which decays to leptons but not hadrons.

Theories have also been proposed that explain the discrepancy between the DM-like signal at DAMA/LIBRA and the apparent lack of signals at other DM searches. In the eXciting Dark Matter (XDM) scenario [13], the WIMP has an excited state $\mathcal{O}(1$ MeV) above the ground state. Collisions between WIMPs can proceed by the interaction $\chi\chi \to \chi\chi^*$, and the resulting excitation subsequently decays via $\chi^* \to \chi e^+e^-$ through a mediator like the A'. The size of the mass splitting between χ and χ^* also determines the WIMP's interaction cross section with atomic nuclei, and can be chosen to explain DM signals in some detectors but not others [14].

Most dark sector models include a new scalar, pseudoscalar, or spin-1 field to carry out the functions described above (the dark photon is the latter case). In order to provide observable signals, a coupling must exist, albeit weak, between the SM and the dark sector. A scalar field ϕ can couple to the SM gauge or Higgs sector with terms of the form $\phi F^{\mu\nu}F_{\mu\nu}$ or $\kappa\phi^2 h^\dagger h$. The former case results in photon and gluon production; the latter can result in a vev $\langle\phi\rangle \sim m_\phi$ which produces a small mixing with the SM Higgs and results in a coupling to the heaviest allowable fermion pair. The possibility of a pseudoscalar field is not favored in [12] because it leads to a long-range spin-dependent potential which vanishes when averaged over all angles. This has the effect of cancelling any Sommerfeld enhancement in s-wave interactions. Finally, a spin-1 field A' can mix with electromagnetism via $\epsilon F^{\mu\nu}F'_{\mu\nu}$, a scenario first explored in [15]. Here, the A' is a $U(1)$ gauge field that couples directly to charge, allowing for the direct decay to leptons $A' \to \ell^+\ell^-$.

We expand on the spin-1 case by writing out the relevant terms for the *kinetic mixing* of

$U(1)_Y \times U(1)_{\text{dark}}$. In the gauge eigenbasis, we have [16]:

$$\mathcal{L}_{\text{gauge mix}} = -\frac{1}{4} W_{3\mu\nu} W_3^{\mu\nu} - \frac{1}{4} B_{\mu\nu} B^{\mu\nu} + \frac{\epsilon}{2} B_{\mu\nu} A'^{\mu\nu} - \frac{1}{4} A'_{\mu\nu} A'^{\mu\nu} \tag{1}$$

where $W_3^{\mu\nu}$ corresponds to the third generator of $SU(2)$, $B^{\mu\nu}$ is the gauge field for $U(1)_Y$, and $A'^{\mu\nu}$ is the dark $U(1)$ gauge field corresponding to the dark photon A'. After electroweak symmetry breaking, this can be written in the mass eigenbasis:

$$\mathcal{L}_{\text{gauge mix}} = -\frac{1}{4} Z_{\mu\nu} Z^{\mu\nu} - \frac{1}{4} F_{\mu\nu} F^{\mu\nu} - \frac{1}{4} A'_{\mu\nu} A'^{\mu\nu} + \frac{\epsilon}{2} (\cos\theta_W F_{\mu\nu} - \sin\theta_W Z_{\mu\nu}) A'^{\mu\nu} \tag{2}$$

where $F_{\mu\nu}$ and $Z_{\mu\nu}$ are the field strength tensors for the SM photon and Z boson. To expose the interactions generated by the new $U(1)$ field, we can remove the kinetic mixing with a field redefinition on the SM photon:

$$A_\mu \to A_\mu - \epsilon \cos\theta_W A'_\mu. \tag{3}$$

The effect of this redefinition is to couple the dark photon to the electromagnetic current J^μ_{EM} of the SM. The relevant coupling term is given by:

$$\mathcal{L}_{\text{coupling}} = \epsilon \cos\theta_W A'_\mu J^\mu_{\text{EM}} \tag{4}$$

Hence, we obtain the decay $A' \to \ell^+\ell^-$.

The phenomenology outlined above is the simplest model-independent consequence of the mixing $U(1)_Y \times U(1)_{\text{dark}}$. However, more complicated signatures can also arise. Coupling to the SM Z boson via a similar mechanism can produce rare Z decays to dark sector particles. Also, kinetic mixing can be extended into the SUSY sector, generating electroweakino decays that produce boosted A's. Finally, there can be a coupling between the Higgs and dark sectors. The experimental signatures of these processes usually involve *lepton jets* stemming from the boosted decays $A' \to \ell^+\ell^-$. Searches for events containing lepton jets are currently ongoing at the LHC experiments.

4 Future Experimental Prospects

The possible existence of a GeV-scale dark photon has exciting prospects for experiments on the intensity frontier. The ϵ-$m_{A'}$ parameter space has already been probed by high-intensity beam dump experiments and constrained by measurements in astrophysics and precision QED. Several new experiments will soon be underway to further extend our reach. The general strategy for collider-based dark photon searches is to observe the decay $A' \to \ell^+\ell^-$ or $A' \to$ invisible. The parameter space for these decays is shown in Figure 4 along with current and projected experimental constraints. Here we focus on the region of parameter space above $m_{A'} \sim 2m_e$ that is accessible to collider experiments.

Beam dump experiments at SLAC, Fermilab, KEK, and Orsay exclude the region at the left and bottom of Figure 4(a). In this kinematic regime, a highly-boosted A' is produced and

travels through a shield to separate it from SM backgrounds. The reach of these experiments is determined by the available integrated luminosity, as well as the beam energy, shield length, and distance between the beam dump and detector. At higher values of $m_{A'}$, the dark photon decays more quickly and more sophisticated techniques are needed to distinguish A' production from SM processes.

New measurements have been proposed at e^+e^- and fixed-target colliders, as well as Tevatron and LHC experiments. Together, they will probe the many challenging regions of the ϵ-$m_{A'}$ parameter space. The various regions of the parameter space are roughly defined by the A' lifetime, determined by $m_{A'}$ and ϵ, and its production cross section which is determined primarily by ϵ. The lifetime of the A' can be approximated by [17]:

$$c\tau \simeq \frac{3}{N_{\rm eff} m_{A'} \alpha \epsilon^2} \tag{5}$$

where $N_{\rm eff}$ is the number of available decay products for the A'. As $m_{A'}$ increases above the beam-dump regime, large displacements are no longer observed in A' decays, except at very-low ϵ. Furthermore, the value of ϵ dictates the rate of A' production with respect to SM processes. In the low-ϵ region, the A' lifetime is large enough to enable some separation from SM backgrounds, even though the production rate is highly suppressed. High-energy colliders are not optimal for A' searches due to a high rate of SM backgrounds. However, efforts are ongoing to look for specific signatures involving "lepton-jets" which might result from highly-boosted A' production. Although sensitivity to these scenarios can be obtained, these measurements are less generic and include model assumptions. Below, we discuss some of the proposed and ongoing searches for a GeV-scale dark photon.

4.1 e^+e^- Colliders

The prospects for dark boson searches at e^+e^- experiments are discussed in [18]. Here, both direct production and rare meson decays are considered. In the former case, the interaction $e^+e^- \to \gamma A'$ is similar to the standard model version, $e^+e^- \to \gamma\gamma$, with a rate suppressed by a factor of ϵ^2. The primary physics background is the production of a virtual photon, $e^+e^- \to \gamma\gamma^* \to \gamma\ell^+\ell^-$, with $q_{\gamma^*} \sim m_{A'}$. The reach is given by computing the relevant cross sections from QED:

$$\frac{S}{\sqrt{B}} \sim \sqrt{\sigma_0 \mathcal{L}} \frac{\epsilon^2}{\sqrt{\alpha/\pi}} \sqrt{\frac{m_{A'}}{\delta m}} \times {\rm BR}(A' \to \ell^+\ell^-) \tag{6}$$

where $\delta m \approx 1$ MeV is the approximate resolution on $m_{\ell^+\ell^-}$, $\sigma_0 \sim 1 \times 10^7$ pb is roughly the cross-section for $e^+e^- \to \gamma\gamma$, and $\mathcal{L}$ is the integrated luminosity. It is apparent from this estimate that our reach on ϵ goes as $\mathcal{L}^{-1/4}$. This poses a considerable challenge in exploring the low-ϵ regions of parameter space – we have a statistics-limited measurement where large gains in the luminosity have a mediocre effect on the outcome. For example, an order of magnitude increase in $\mathcal{L}$ gives only a 25% increase in our reach on ϵ. A search down to $\epsilon \sim 10^{-4}$ in this scenario would require $\mathcal{L} \sim 1$ ab^{-1} of integrated luminosity, which

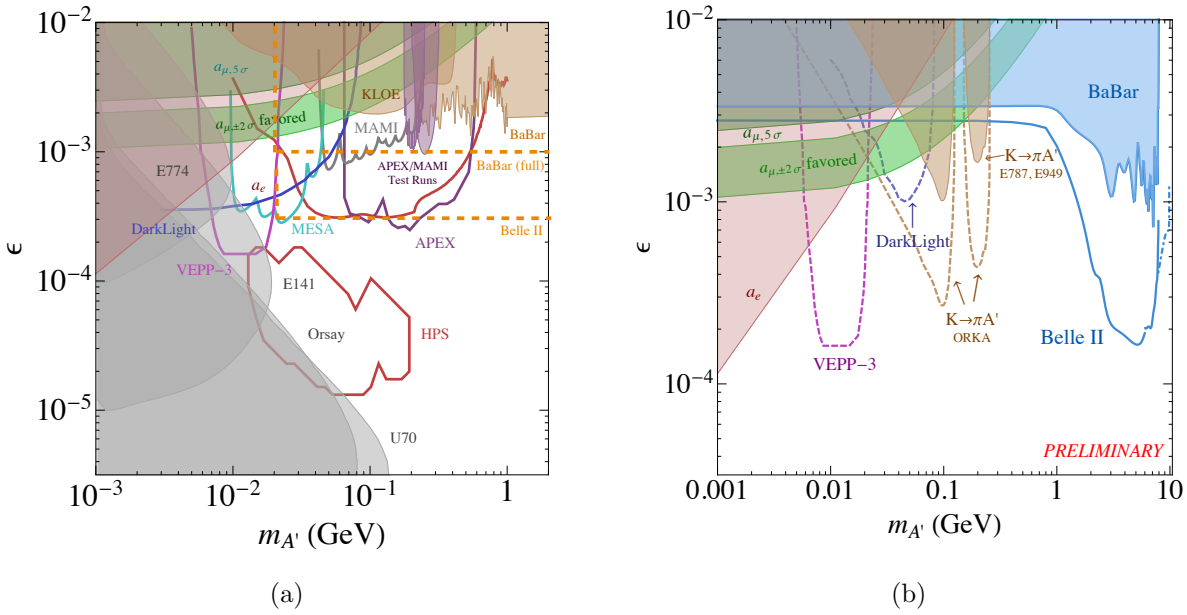

Figure 4: The ϵ-$m_{A'}$ parameter space with current constraints and projected reach from a variety of experiments. Visible decays of the A' are shown at the right, and invisible decays at the left.

is roughly the size of the current BaBar and Belle datasets. For more competitive limits, significant enhancements to the luminosity are required.

Searches have been proposed using the data collected at the BaBar and Belle B-factories [19] which utilize the strategy outlined above. At BaBar, a 9 GeV electron beam is incident on a 3.1 GeV positron beam; Belle utilizes an 8 GeV electron beam and 3.5 GeV positron beam. Both detectors allow for full event reconstruction. The BaBar and Belle experiments have obtained about 500 and 1000 fb^{-1} of e^+e^- data at around the $\Upsilon(4S)$ resonance, respectively. In addition to this, the planned Belle II experiment is scheduled to collect 50 ab^{-1} of data by 2022. An estimate of the reach on ϵ using 432.89 fb^{-1} of BaBar data is conducted in [18] and reproduced in Figure 5. Signal events are generated with simple Monte Carlo simulation based on an estimate of $d\sigma/d\cos\theta$ in the process $e^+e^- \to A'\gamma$ with $A' \to \ell^+\ell^-$. Backgrounds are simulated in MadGraph and estimates are included for the mass resolution of e^+e^-, $\mu^+\mu^-$, and $\pi^+\pi^-$ decays in the BaBar detector. A degradation of the reach is obtained near the ρ resonance due to the increased $A' \to \pi^+\pi^-$ branching fraction, but this is partially recovered by introducing the $\pi^+\pi^-$ channel into the measurement. The reach shown in this study extends down to $\epsilon \sim 1 \times 10^{-3}$ over a range of masses $m_{A'}$. Scaling this by the 100-fold increase in the expected Belle II dataset, the sensitivity on ϵ can be increased by a factor of 3. Additional improvements can also be obtained depending on backgrounds and detector performance.

Meson decays involving a dark photon occur via the same mechanism as the standard model decay, with $\mathrm{BR}(X \to Y + A') \approx \epsilon^2 \mathrm{BR}(X \to Y + \gamma)$. The dominant background for

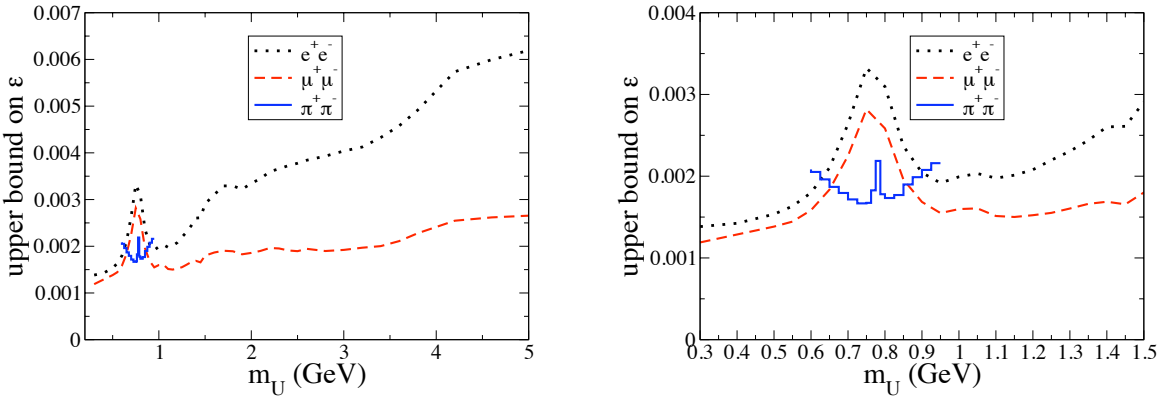

Figure 5: Reach on ϵ at BaBar with 432.89 fb^{-1} of e^+e^- data in three channels with e^+e^-, $\mu^+\mu^-$, and $\pi^+\pi^-$ in the final state. A ratio $S/\sqrt{B} = 5$ is assumed. The mass range $0 < m_{A'} < 5$ GeV is shown at the left; on the right, the region near the ρ resonance is enlarged. The decreasing sensitivity at high $m_{A'}$ observed in the e^+e^- channel can be attributed to the increase in Bhabha scattering events.

such processes is the decay $X \to Y + \gamma^*$ with $q_{\gamma^*} = m_{A'}$. The reach can be estimated from the QED by:

$$\frac{S}{\sqrt{B}} \sim \sqrt{n_X}\frac{\epsilon^2 \times \mathrm{BR}(X \to Y + \gamma) \times \mathrm{BR}(U \to \ell^+\ell^-)}{\sqrt{\mathrm{BR}(X \to Y + \gamma^8 \to Y + \ell^+\ell^-)}}\sqrt{\frac{m_{A'}}{\delta m}\log\left(\frac{m_X - m_Y}{2m_\ell}\right)} \qquad (7)$$

where n_X is the number of mesons produced. Here again we have the dependence $\epsilon \propto n_X^{-1/4}$ so that $n_X \sim O(10^9)$ is needed to reach $\epsilon \sim 10^{-3}$. Estimates on the reach for a variety of channels are presented in Table 1 of [18]. In particular, a search strategy is proposed in ϕ decays at the KLOE experiment, which has collected 2.5 fb^{-1} of data, or approximately 8 billion ϕ mesons at a center of mass energy of 1.02 GeV. The KLOE-2 experiment is expected to expand on this by collecting O(20 fb^{-1}) with an improved detector, providing a factor of 3-5 increase in sensitivity. The proposed decay channel is $\phi \to \eta\gamma$, which occurs 1.3% of the time. The η meson then decays to diphotons 39% of the time. The relevant search modes are $\phi \to \eta A'$ or $\phi \to \eta\gamma \to \gamma\gamma A'$. The reach as a function of $m_{A'}$ is shown in Figure 6. The reach here is similar to that obtained from BaBar data – approximately $\epsilon \sim 2 \times 10^{-3}$ at $m_{A'} = 214$ MeV.

4.2 *ep* (Fixed Target) Colliders

The high luminosities available at fixed target experiments make them very attractive for probing the ϵ-m_A parameter space. In electron collisions with an atomic nucleus, the A' is produced in a process similar to photon bremsstrahlung. The cross section for this process can be approximated by $\sigma \propto \alpha^3\epsilon^2 Z^2/m_{A'}^2 \propto 1$ pb. This is a significant improvement over

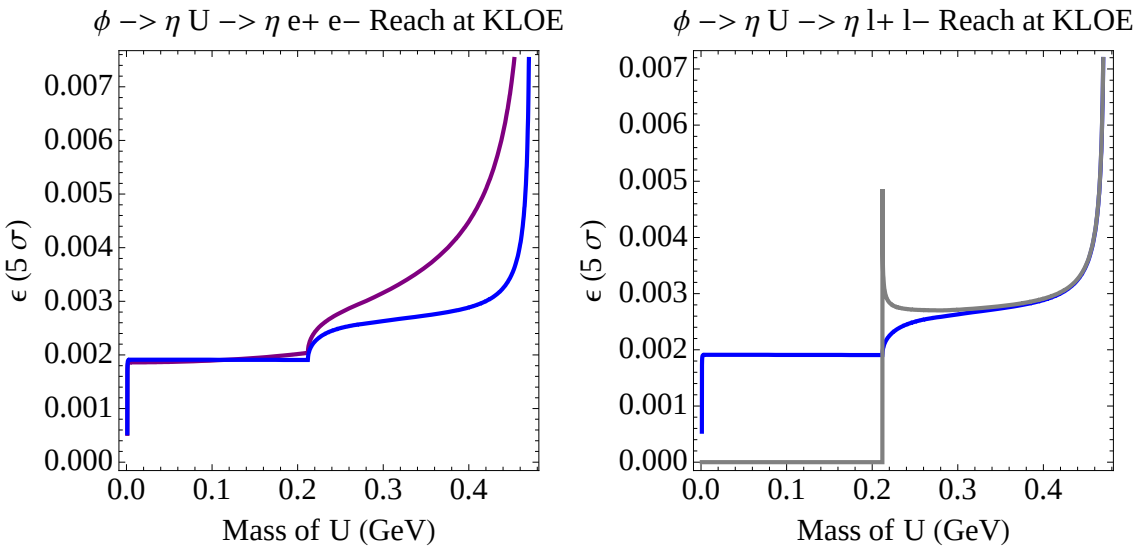

Figure 6: Reach on ϵ in the decay $\phi \to \eta A'$. The curves represent different form factors used in the cross section calculation. The kink near 0.2 GeV occurs when the decay $A' \to \mu^+\mu^-$ becomes kinematically plausible. The decay to two pions turns on at 0.28 GeV, but the branching fraction remains small and it has little effect on the reach.

the $e^+e^- \to \gamma A'$ cross section, $\sigma \propto \alpha^2\epsilon^2/E_{CM}^2 \propto 1$ fb [20] offered by e^+e^- experiments. In other words, the number of A' particles after a decade of e^+e^- collisions can be created at a fixed-target experiment in one day.

In addition to the boost in luminosity obtained at fixed-target experiments, A' production in ep collisions has kinematics which allows for good discrimination from ordinary bremsstrahlung [17, 20, 21]. The differential cross section for A' production scales as

$$\frac{d\sigma}{dx} \propto \frac{\alpha^3}{\pi} \frac{\epsilon^2}{m_e^2 \cdot x + m_{A'}^2(1-x)/x} \tag{8}$$

where $x = E_{A'}/E_{\text{beam}}$. This distribution peaks at $x \approx 1$ where the A' takes most of the beam energy. The A' is thus boosted in the forward direction, with the recoiling electron emitted at a larger angle from the beam line. The decay products of the A' are also boosted, partially due to the mass of the A', and occur in the forward region. An illustration of this is reproduced from [21] in Figure 7. The analogous kinematics in photon bremsstrahlung can be obtained by setting $m_{A'} = 0$ in Equation 8. Here, the rate falls with increasing x, producing low-energy photons emitted at large angles and recoiling electrons in the forward region.

A number of experiments have been proposed to take advantage of these features. Among these are three experiments at Jefferson Laboratory (JLab) – HPS, DarkLight and APEX – an experiment at the VEPP-3 storage ring in Novosibirsk, and a 3-phase program at Mainz in Germany. The projected reach of these experiments extends down to $\epsilon \sim 10^{-5}$ and A'

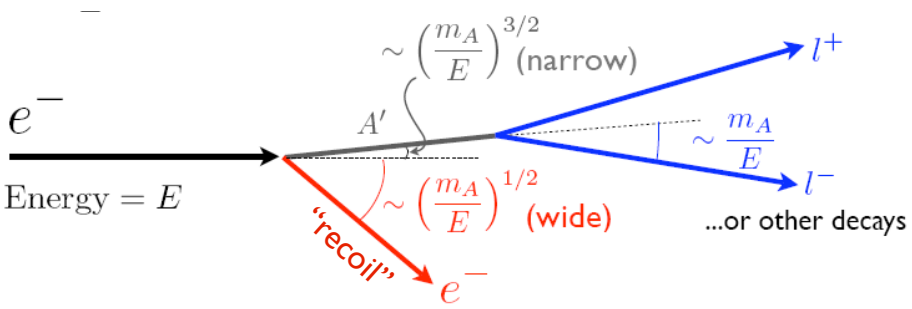

Figure 7: An illustration of the kinematics of A' production at ep colliders [21]. The A' is preferentially emitted in the forward direction, carrying the majority of the beam energy. The resulting dilepton pair is observed preferentially in the forward direction.

masses up to several GeV. The dominant backgrounds are due to photon bremsstrahlung and Bethe-Heitler trident production. We give a concise overview below.

HPS (Heavy Photon Search): a forward-vertexing spectrometer The HPS experiment [22] will scan over a broad range of masses, $20 < m_{A'} < 1000$ MeV, utilizing beams of energies 2.2 GeV and 6.6 GeV incident on a tungsten (W) target of width 0.15%-0.25% radiation lengths. The detector layout includes a Si tracking and vertexing system directly downstream from the target and inside a magnetic field. Further down the beamline are positioned an electromagnetic calorimeter and muon system for triggering and particle ID. The A' search will proceed via two avenues – a resonance search and displaced vertex search. In the former, the A' will produce a bump in the dilepton invariant mass. This measurement will be statistics (background) and mass-resolution limited and will probe a region of large ϵ. The latter will be sensitive to A' bosons with a smaller ϵ, and backgrounds are highly suppressed. It is limited by luminosity and acceptance for A' with large lifetimes.

APEX (A Prime EXperiment): dual-arm spectrometers The APEX experiment [23,24] is planning to search in mass range $65 < m_{A'} < 525$ GeV by using a 12 GeV beam from the CEBAF machine, incident on a 50cm long tantalum (Ta) multifoil target. The search region accessible by APEX largely overlaps with HPS, but the experimental strategy is aimed at a very precise reconstruction of $m_{e^+e^-}$, with a relative momentum resolution of $O(10^{-4})$. The experimental setup includes two septum magnets to bend the e^+/e^- trajectories at angles of 5deg relative to the incident beam into two high resolution spectrometers. This configuration takes advantage of the kinematics involved in A' production – the opening angle for signal e^+e^- pairs is expected to be $\Theta \sim m_{A'}/E_b \approx 5^\circ$ [20]. The dominant contributions to the mass resolution are the angular resolution and multiple scattering in the target.

DarkLight: gaseous target with full final state reconstruction The DarkLight (Detecting A Resonance Kinematically with eLectrons Incident on a Gaseous Hydrogen Target) experiment [25, 26], proposed to be position at the FEL (Free Electron Laser) at

JLab, takes the approach of a 100 MeV electron beam on a Hydrogen gas target. The high intensity available at the FEL will deliver an integrated luminosity of 1 ab^{-1} after 1-2 months of running. The accessible mass range will be $10 < m_{A'} < 90$ GeV. The detector at DarkLight will include full reconstruction of the four particle final state, which gives it the advantage of imposing strong kinematic constraints for background rejection. In addition to this, DarkLight provides photon identification for better rejection of SM backgrounds. As a result, DarkLight has sensitivity to the decay $A' \rightarrow$ invisible in addition to the dileptonic decay.

MAMI/MESA: a 3-phase program A proposal for a dark photon search at University of Mainz in Germany outlines a 3-phase program for probing a broad region of the parameter space [27]. The first two phases make use of the electron beam at the MAMI accelerator, with possible beam energies in the range $180 < E_b < 720$ MeV. The first stage will include two high resolution spectrometers to provide $O(10^{-4})$ relative momentum resolution for good dielectron mass reconstruction. The beam is incident on a target of 12 strips of tantalum (Ta) foil. This will probe the high-ϵ, high-mass region of parameter space. For reach into the low-ϵ region, phase II will focus on vertex reconstruction with two angular acceptance spectrometers. In phase III, the experiment will move to the MESA accelerator with a beam energy of 200 MeV, and will operate in an ERL (Electron Recovery Linac) mode with an internal gas target as well as an extracted beam mode. This final stage is expected to probe the low-mass, low-ϵ region of parameter space.

VEPP-3: positron beam on a gaseous target The proposed experiment at VEPP-3 in Novosibirsk differs from most other fixed-target experiments in that a 500 MeV *positron* beam is incident on a Hydrogen gas target [28]. Here the relevant interaction is $e^+e^- \rightarrow \gamma A'$, where beam particles annihilate with electrons in the Hydrogen. The experimental technique requires only a measurement of the photon energy E_γ and angle Θ_γ. The A' signal appears as a band in the Θ_γ-E_γ plane above the continuum of SM processes including bremsstrahlung of the beam positrons against electrons or protons in the target, and photons from the three-photon annihilation process. Because the decay products of the A' are not reconstructed, this experiment has sensitivity to dileptonic as well as invisible A' decays.

4.3 TeV-Scale Probes

Experiments at the TeV scale are typically sensitive to dark sectors through complex decay chains rather than simple dileptonic signatures. In particular, the possibility of lepton jets was first suggested in [29] as a consequence of embedding the dark sector within low-energy SUSY. Lepton jets arise from boosted $A' \rightarrow \ell^+\ell^-$ production in cascade decays of MSSM superpartners as well as rare decays of the SM Z and Higgs bosons (Figure 8). They contain at least two leptons with a small opening angle and order-GeV invariant mass. Often, lepton jet signatures also also accompanied by MET due to invisible decays of dark sector particles.

Searches for dark sectors have been conducted at the Tevatron and LHC experiments [31].

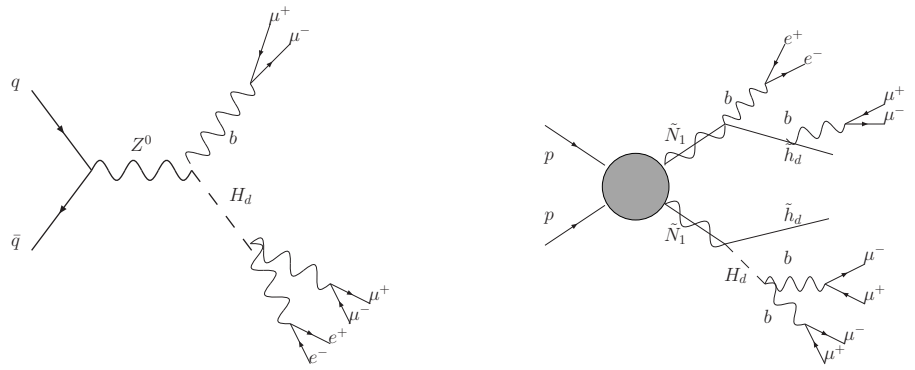

Figure 8: Production of lepton jets at the LHC [30].

Recently, the CMS experiment has searched for Higgs bosons [32] and light resonances [33] decaying to muon jets in 7 TeV data. CMS has approached muon jet reconstruction by identifying individual muons with an $\mathcal{O}(1$ GeV) invariant mass. A muon jet signal appears as an excess in the dimuon invariant mass spectrum from isolated muon pairs. In the Higgs analysis, two muon jets are required within some invariant mass threshold of each other. In the search for light resonances, topologies include 1 dimuon jet, 2 dimuon jets, and 1 quadmuon jet were considered. CMS also has sensitivity to displaced vertices up to ∼40cm from the beamline. No excesses were identified in these searches, and appropriate limits were set. Decays of the SM Higgs with an approximately 1% branching ratio to muon jets have been excluded.

The ATLAS experiment has searched for events with lepton jets resulting from both prompt [34] and Higgs [35,36] decays at 7 TeV. ATLAS has approached electron jet searches with custom reconstruction based on several discriminating variables which use tracker and calorimeter information. For the reconstruction of muon jets, an iterative seeding procedure is used. Limits were set on prompt dark photon production with decays to two prompt lepton jets containing either muons or electrons, and events with one prompt 4-muon lepton jet [34]. A limit for SM WH Higgs production with the Higgs decaying to electron jets was set at about 50% of the SM production cross section. Finally, in a search for displaced muon jets resulting from a light Higgs decay, limits were obtained on the cross section for displaced vertices up to ∼50 cm.

The reach of the LHC experiments on $m_{A'}$ is determined primarily by the reconstruction capabilities of the CMS and ATLAS detectors. Muon reconstruction in both experiments has so far allowed for sensitivity down to $m_{\mu\mu} \sim 250$ MeV. At ATLAS, the sensitivity to electron jets extends down to $m_{ee} \sim 150$ MeV. The reach of these experiments in ϵ is difficult to quantify, largely because the searches make model assumptions beyond the simple decay of an A'. The search results are typically interpreted in terms of simplified models that can be applied to a variety of physics scenarios.

The LHC experiments will continue to probe for dark sector interactions as larger datasets at 13 TeV become available. In addition to the increase in statistics, it will be beneficial to

improve the reconstruction of lepton jets and explore a wider variety of signatures. Many of the signatures probed at the LHC assume a dark sector that couples to SUSY or Higgs sectors. Although not as generic, these searches will complement the efforts at lower energy e^+e^- and fixed-target experiments.

5 Conclusions

We have seen that a collection of evidence from measurements of high-energy cosmic rays, gamma rays, and microwaves, as well as terrestrial DM searches, motivates a dark sector explanation for DM. The dark photon is a candidate dark sector particle which loosely mixes with electromagnetism in the SM. There is now an ongoing effort to search for dark photons in collider-based experiments on the intensity frontier. This exciting new experimental program will provide useful input to the new physics searches currently taking place at the LHC and cosmic-frontier.

Acknowledgements I would like to thank my committee, Jim, Peter, and Maxim, for giving me the opportunity to learn more about these fascinating topics on the cutting edge of fundamental physics. Thank you also to Mike Saelim and Brian Koopman for helpful discussions about kinetic mixing and the CMB.

References

[1] I. V. Moskalenko and A. W. Strong. Production and Propagation of Cosmic-Ray Positrons and Electrons. *Astrophys. J.*, 493:694, January 1998.

[2] O. Adriani et al. The cosmic-ray positron energy spectrum measured by pamela. August 2013.

[3] Fermi LAT Collaboration. Measurement of separate cosmic-ray electron and positron spectra with the fermi large area telescope. *Phys. Rev. Lett.*, 108:011103, Jan 2012.

[4] AMS Collaboration. First result from the alpha magnetic spectrometer on the international space station: Precision measurement of the positron fraction in primary cosmic rays of 0.5˘350 gev. *Phys. Rev. Lett.*, 110:141102, Apr 2013.

[5] J. Chang et al. An excess of cosmic ray electrons at energies of 300-800 gev. *Nature*, 456:362365, November 2008.

[6] A.W. Strong, R. Diehl, H. Halloin, V. Schnfelder, L. Bouchet, P. Mandrou, F. Lebrun, and R. Terrier. Gamma-ray continuum emission from the inner galactic region as observed with integral/spi. *Astronomy and Astrophysics*, 444(2):495–503, December 2005.

[7] E. Churazov, R. Sunyaev, S. Sazonov, M. Revnivtsev, and D. Varshalovich. Positron annihilation spectrum from the galactic centre region observed by spi/integral. *Mon. Not. Roy. Astron. Soc.*, 357:13771386, December 2005.

[8] Douglas P. Finkbeiner. Microwave interstellar medium emission observed by the wilkinson microwave anisotropy probe. *The Astrophysical Journal*, 614(1):186, 2004.

[9] The wmap haze excess and wimp annihilations.

[10] R. Bernabei, P. Belli, and A. Di Marco. Dama/libra results and perspectives. January 2013.

[11] CDMS Collaboration. Silicon detector dark matter results from the final exposure of cdms ii. October 2013.

[12] Nima Arkani-Hamed, Douglas P. Finkbeiner, Tracy R. Slatyer, and Neal Weiner. A theory of dark matter. *Phys. Rev. D*, 79:015014, Jan 2009.

[13] Douglas P. Finkbeiner and Neal Weiner. Exciting dark matter and the integral/spi 511 kev signal. *Phys. Rev. D*, 76:083519, Oct 2007.

[14] David Smith and Neal Weiner. Inelastic dark matter. *Phys. Rev. D*, 64:043502, Jul 2001.

[15] Bob Holdom. Two u(1)'s and charge shifts. *Physics Letters B*, 166(2):196 – 198, 1986.

[16] Matthew Baumgart, Clifford Cheung, Joshua T. Ruderman, Lian-Tao Wang, and Itay Yavin. Non-abelian dark sectors and their collider signatures. *Journal of High Energy Physics*, 2009(04):014, 2009.

[17] James D. Bjorken, Rouven Essig, Philip Schuster, and Natalia Toro. New fixed-target experiments to search for dark gauge forces. *Phys. Rev. D*, 80:075018, Oct 2009.

[18] Matthew Reece and Lian-Tao Wang. Searching for the light dark gauge boson in gev-scale experiments. *Journal of High Energy Physics*, 2009(07):051, 2009.

[19] Bertrand Echenard. Hidden sector searches at e^+e^- colliders. Snowmass 2013.

[20] Rouven Essig. Probing dark forces with low energy e^+e^- colliders, new fixed-target experiments, and dwarf galaxies. Fermilab Theory Seminar, November 2009.

[21] Tim Nelson. Thoughts on future heavy photon searches. Snowmass 2013.

[22] A. Grillo et al. Hps heavy photon search: A proposal to search for massive photons at jefferson laboratory. December 2010.

[23] Rouven Essig, Philip Schuster, Natalia Toro, and Bogdan Wojtsekhowski. An electron fixed target experiment to search for a new vector boson a' decaying to e^+e^-. *Journal of High Energy Physics*, 2011:001035, February 2011.

[24] James Beacham. Apex: A prime experiment at jefferson lab. January 2013.

[25] J. Balewski et al. A proposal for the darklight experiment at the jefferson laboratory free electron laser. PAC39, May 2012.

[26] Marat Freytsis, Grigory Ovanesyan, and Jesse Thaler. Dark force detection in low energy e-p collisions. October 2009.

[27] Achim Denig. Dark photon searches at mami and mesa. PATRAS Conference Mainz, June 2013.

[28] D. B. Wojtsekhowski and I.R. Nikolenko. Searching for a new force at vepp-3. July 2012.

[29] Nima Arkani-Hamed and Neal Weiner. Lhc signals for a superunified theory of dark matter. *Journal of High Energy Physics*, 2008(12):104, 2008.

[30] Clifford Cheung, JoshuaT. Ruderman, Lian-Tao Wang, and Itay Yavin. Lepton jets in (supersymmetric) electroweak processes. *Journal of High Energy Physics*, 2010(4):1–23, 2010.

[31] Andy Haas. Hidden sector particles at the lhc. Intensity Frontier Workshop, Argonne, April 2013.

[32] CMS Collaboration. Search for a non-standard-model higgs boson decaying to a pair of new light bosons in four-muon final states.

[33] CMS Collaboration. Search for light resonances decaying into pairs of muons as a signal of new physics. *Journal of High Energy Physics*, 2011(7):1–34, 2011.

[34] ATLAS Collaboration. A search for prompt lepton-jets in pp collisions at with the ATLAS detector. *Physics Letters B*, 719(45):299 – 317, 2013.

[35] ATLAS Collaboration. Search for wh production with a light higgs boson decaying to prompt electron-jets in protonproton collisions at $\sqrt{s} = 7$tev with the atlas detector. *New Journal of Physics*, 15(4):043009, 2013.

[36] Search for displaced muonic lepton jets from light higgs boson decay in protonproton collisions at with the ATLAS detector. *Physics Letters B*, 721(13):32 – 50, 2013.